EVIDENCE OF THE SOLAR EUV HOT CHANNEL AS A MAGNETIC FLUX ROPE FROM REMOTE-SENSING AND IN SITU OBSERVATIONS

H. Q. SONG[1], Y. CHEN[1], J. ZHANG[2], X. CHENG[3], B. WANG[1], Q. HU[4], G. LI[4], AND Y. M. WANG[5]

[1] Shandong Provincial Key Laboratory of Optical Astronomy and Solar-Terrestrial Environment, and Institute of Space Sciences, Shandong University, Weihai, Shandong 264209, China; hqsong@sdu.edu.cn
[2] School of Physics, Astronomy and Computational Sciences, George Mason University, Fairfax, VA 22030, USA
[3] School of Astronomy and Space Science, Nanjing University, Nanjing, Jiangsu 210093, China
[4] Department of Space Science and CSPAR, University of Alabama in Huntsville, Huntsville, AL 35899, USA
[5] Key Laboratory of Geospace Environment, University of Science and Technology of China, Chinese Academy of Sciences (CAS), Hefei, Anhui 230026, China

ABSTRACT

Hot channels (HCs), high-temperature erupting structures in the lower corona of the Sun, have been proposed as a proxy of magnetic flux ropes (MFRs) since their initial discovery. However, it is difficult to provide definitive proof given the fact that there is no direct measurement of the magnetic field in the corona. An alternative method is to use the magnetic field measurement in the solar wind from in situ instruments. On 2012 July 12, an HC was observed prior to and during a coronal mass ejection (CME) by the Atmospheric Imaging Assembly high-temperature images. The HC is invisible in the EUVI low-temperature images, which only show the cooler leading front (LF). However, both the LF and an ejecta can be observed in the coronagraphic images. These are consistent with the high temperature and high density of the HC and support that the ejecta is the erupted HC. Meanwhile, the associated CME shock was identified ahead of the ejecta and the sheath through the COR2 images, and the corresponding ICME was detected by the *Advanced Composition Explorer*, showing the shock, sheath, and magnetic cloud (MC) sequentially, which agrees with the coronagraphic observations. Further, the MC average Fe charge state is elevated, containing a relatively low-ionization-state center and a high-ionization-state shell, consistent with the preexisting HC observation and its growth through magnetic reconnection. All of these observations support that the MC detected near the Earth is the counterpart of the erupted HC in the corona for this event. The study provides strong observational evidence of the HC as an MFR.

Key words: magnetic reconnection – Sun: coronal mass ejections (CMEs) – Sun: flares

Supporting material: animations

1. INTRODUCTION

Coronal mass ejections (CMEs), the most energetic eruptions in the solar system, can cause geomagnetic activities when they interact with the Earth's magnetosphere (Gosling et al. 1991; Zhang et al. 2003, 2007), which will affect and even damage the satellites, power grids, and GPS navigation systems. Currently, the solar physics community has reached a general consensus that CMEs are associated with the eruption of magnetic flux ropes (MFRs; e.g., Chen 2011; Cheng et al. 2013, 2014a). The in situ detections of magnetic clouds (MCs) contained in the interplanetary CMEs (ICMEs; Burlaga et al. 1981) provide direct evidence of the existence of MFRs. In the outer corona, at least ∼40% of coronagraphic observations of CMEs show an apparent MFR geometry (Vourlidas et al. 2013), further supporting that the CME structures contain MFRs. It is believed that MFRs should exist in the inner corona, either forming before (Patsourakos et al. 2013) or during (Song et al. 2014a) the eruptions. However, it is still an open question of what structures really depict the MFRs in the inner corona as we do not have the direct measurements of the coronal magnetic fields yet.

In addition to sigmoids (Titov & Démoulin 1999; McKenzie & Canfield 2008) and coronal cavities (Wang & Stenborg 2010), which are widely regarded as proxies of the MFRs in the inner corona, Zhang et al. (2012) first reported and suggested that a new observational line, hot channels (HCs), is the MFR in the inner corona. HCs refer to the high-temperature

structure revealed first by the Atmospheric Imaging Assembly (AIA) 131 Å passband (sensitive to ∼10 MK) and are invisible in the cooler temperature images (e.g., AIA 171 Å passband, sensitive to ∼0.6 MK). An HC will appear as a hot blob when observed along its axis due to the projection effect (Cheng et al. 2011; Patsourakos et al. 2013; Song et al. 2014a, 2014b). Since the discovery of HCs, some evidence has been reported to support that they might be the MFRs. For instance, Cheng et al. (2014a) presented an HC with helical threads winding around an axis, which indicates the intrinsic helical structure of HC; Cheng et al. (2011) found that an HC can grow during the eruption, consistent with the MFR growth process in the classic magnetic reconnection scenario. This further supports that an HC is the MFR structure; Cheng et al. (2014b) reported that an HC was cospatial with a prominence, while the HC top separated from that of the prominence during the eruption, which offered new evidence that the HC is an MFR, as it is generally accepted that a prominence can exist at the dip of an MFR (Rust & Kumar 1994).

Though many studies indicate that HCs are the MFRs, the direct observational evidence remains lacking. As MFRs are the volumetric plasma structure with magnetic field lines wrapping around an axis, the substantial evidence that supports a structure being the MFR should be based on its measurements of the magnetic fields. However, no reliable measurements of the coronal magnetic fields are available at present, as mentioned. Therefore, we anticipate studying the magnetic fields of HCs through the in situ detections of their

interplanetary counterparts, which might provide strong observational evidence that HCs have the structure of helical fields.

In this Letter, a CME induced by an HC eruption and its associated ICME are investigated. We will provide evidence to establish the HC–MC correspondence. The instruments and methods are introduced in Section 2, and the relevant observations and results are described in Section 3. Section 4 presents the discussion, and Section 5 is a summary.

2. INSTRUMENTS AND METHODS

The eruption process in the lower corona was recorded by the AIA telescope (Lemen et al. 2012) on board the *Solar Dynamic Observatory* (*SDO*) and the Extreme Ultraviolet Imager (EUVI) on board the *Solar Terrestrial Relations Observatory* (*STEREO*) A and B from three different perspectives. AIA has four telescopes to observe the solar atmosphere through 10 narrow UV and EUV passbands with a high cadence (12 s), a high spatial resolution (1″.2), and a large field of view (FOV; 1.3 $R_\odot$). The EUVI provides the solar EUV images at four wavelengths. The related CME was observed with the white-light coronagraphs on board *STEREO*, including COR1 (FOV: 1.4–4 $R_\odot$) and COR2 (FOV: 2.5–15 $R_\odot$; Howard et al. 2008). Near the Earth, the ICME was detected by the *Advanced Composition Explorer* (*ACE*) satellite. We used the in situ data from MAG (Smith et al. 1998), SWEPAM (McComas et al. 1998), and SWICS (Gloeckler et al. 1998) to analyze the solar wind magnetic field and plasma properties. The soft X-ray (SXR) data are from the *Geostationary Operational Environment Satellite* (*GOES*). *GOES* provides the integrated full-disk SXR emission from the Sun, which is used to define the magnitude, onset time, and peak time of solar flares.

The AIA has a broad temperature coverage from 0.6 to 20 MK (O'Dwyer et al. 2010; Del Zanna et al. 2011; Lemen et al. 2012) and is ideal for constructing the differential emission measure (DEM) models of the coronal structures (e.g., Cheng et al. 2012). A DEM-weighted average temperature is used to analyze the HC's initial thermal evolution (see Cheng et al. 2012; Song et al. 2014b).

3. OBSERVATIONS AND RESULTS

3.1. Overview of the Eruption

On 2012 July 12, *GOES* recorded an X1.4 class SXR flare, which was located at the heliographic coordinates S17W08 (NOAA 11520) from the Earth's perspective. The corresponding SXR flux rose gradually from ~14:50 UT, then it started to increase rapidly at ~16:10 UT and peaked at ~16:49 UT.

Cheng et al. (2014c) have analyzed this event and concluded that there were a high-lying MFR (a diffuse and elongated HC) and a low-lying MFR (a sigmoid) coexisting above the same polarity inversion line of the active region for 2 hr prior to the eruption, which formed a double-decker MFR system. Just the high-lying MFR erupted and the associated MC arrived at *ACE* on July 15 at 06:00 UT. This CME propagation process from the Sun to near the Earth has been reported by Möstl et al. (2014) and Hess & Zhang (2014). Shen et al. (2014) presented a data-constrained three-dimensional magnetohydrodynamic simulation for the CME propagation in the corona and interplanetary space, consistent with the observations. Therefore, there is no doubt that the ICME detected with the in situ data corresponds to the CME induced by the HC eruption. We revisit this event to investigate whether or not the detected MC near the Earth is the counterpart of the erupted HC in the corona.

3.2. The HC Eruption and Its Associated CME

When the high-lying HC eruption took place, *STEREO* A and B were 120° west and 115° east of the Earth with distances of 0.96 and 1.02 AU, respectively. As the separation angle is close to 90°, *STEREO* A (B) provides the southeast (southwest) limb view of the eruption as shown in the right (left) panels of Figure 2, while *SDO* presents the disk observation of the active region as presented in Figure 1.

Figure 1(a) is the profile of the *GOES* SXR 1–8 Å flux. The two vertical black lines show the corresponding observation time of the middle and bottom panels, where the AIA 94, 131 Å, and the temperature map obtained through the DEM method are presented in the left, middle, and right panels, respectively. As mentioned, a double-decker MFR system existed in this event. The blue (purple) dotted lines in the middle and bottom panels depict the low (high) lying MFR. Note in panels (b3) and (c3) that the purple line is replaced with the white. The high-lying HC is diffuse and less bright than the flare region, so only the animation of the AIA 94 and 131 Å images accompanying Figure 1 permits the appreciation of the HC's shape and dynamics (also see Cheng et al. 2014c). Usually, the background emissions are less outside the solar disk, and HCs are clearer in the limb events (Zhang et al. 2012; Song et al. 2015). The temperatures of the HC and sigmoid are around 5 MK before the SXR flux began to increase slowly (14:50 UT). After the flare onset, both structures are heated and show obvious temperature enhancement, especially in the sigmoidal region (16:10 UT). As the HC in this event became more diffuse and moved out of the AIA FOV soon after the flare impulsive phase onset, further studies about its growth and heating processes were unavailable. However, it is reasonable to anticipate that the HC will grow up as more poloidal magnetic fluxes injected during the magnetic reconnection (Cheng et al. 2011). In the meantime, its temperature should increase during the flare impulsive phase as expected, likely similar to what happens in a failed HC eruption event (Song et al. 2014b).

The erupting HC shows a writhed morphology with its dominant part lying horizontally from the Earth's perspective. Therefore, the HC was observed edge-on by *STEREO* as shown in Figure 2. However, just the compressed cooler leading front (LF) was recorded (see panels (a) and (b)) by the EUVI 195 Å images (sensitive to ~1.5 MK). As EUVI does not have passbands sensitive to high temperatures, the ejecta is invisible through its images (e.g., 195 Å, see animation (a) accompanying Figure 2), which is consistent with the HC's high temperature. The corresponding CME can be well observed by COR1 as displayed in panels (c) and (d). The coronagraphic images can show the LF and the ejecta/HC clearly as depicted with the arrows because both the compressed region and the HC have a higher density in the corona as compared to the background regions (Cheng et al. 2012; Song et al. 2015). Panels (e) and (f) display the observations of COR2, which also clearly show the LF and the ejecta/HC. (See animation (b) accompanying Figure 2 for the eruption process.) Based on the images recorded by EUVI, COR1, and COR2, we conclude that the ejecta of this CME is a high-temperature and high-
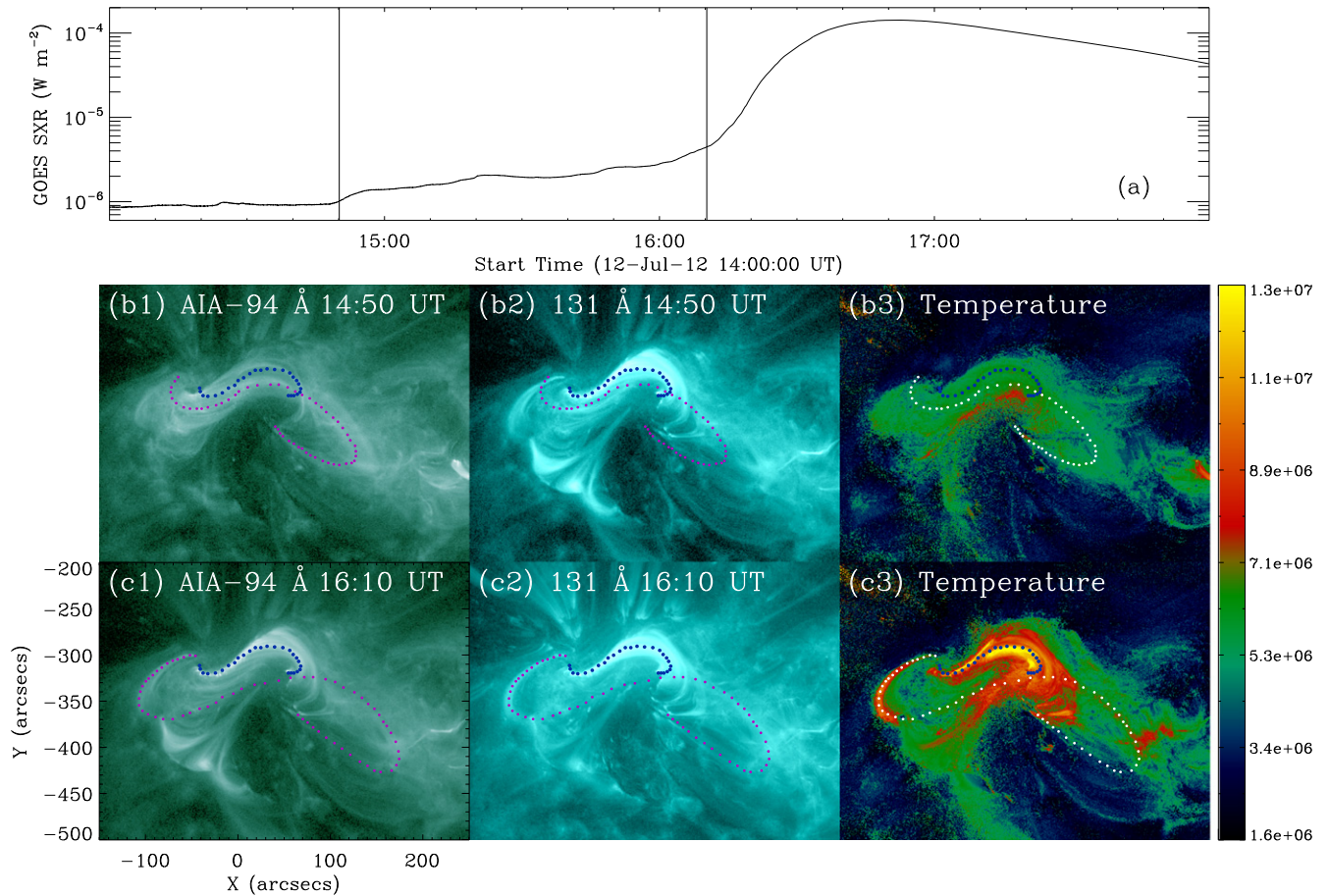
Figure 1. HC eruption event on 2012 July 12. (a) *GOES* SXR 1–8 Å flux profile of the accompanying flare. (b1)–(b3) AIA 94, 131 Å, and temperature image prior to the flare onset. (c1)–(c3) Same as (b1)–(b3), but for a different time.

(An animation of this figure is available.)

density structure, which supports that the ejecta observed by *STEREO* is the HC recorded by *SDO*.

Associated with the CME, an obvious yet diffuse front is generated as depicted with the arrows in Figure 2(f). Generally, the diffuse front ahead of the LF is interpreted as a shock structure (e.g., Vourlidas et al. 2003, 2013; Feng et al. 2012, 2013), and the region between the shock and the HC is usually termed as the sheath. The shock, sheath, and ejecta observed in COR2 images were detected with the in situ observations sequentially as displayed in next subsection.

3.3. The In Situ Detection of the ICME

Figure 3 shows the in situ measurements from the SWEPAM, MAG, and SWICS on board *ACE* at the Lagrangian point (L1). The normalized pitch angle distribution (PAD) of 272 eV electrons (panel (a)), the solar wind speed (black line) and ratios of its three components to the total speed (panel (b)), magnetic field strength (black line) and its three components (panel (c)), proton density and temperature (panel (d)), plasma β and total pressure (panel (e)), and the entropy and average Fe charge state (panel (f)) are displayed from top to bottom. Note the velocity (panel (b)) and magnetic field (panel (c)) components are plotted in the Geocentric Solar Ecliptic coordinate, where the X-axis (red line) points from the Earth toward the Sun, the Y-axis (green line) is chosen to be in the ecliptic plane pointing toward dusk (opposite the Earth's

motion), and the Z-axis (blue line) is parallel to the ecliptic pole.

The shock, sheath, and ejecta (the shaded region) appeared sequentially as expected above. The ejecta part is an MC, with rotations of magnetic field components (especially By, the green line), low temperature and density, as well as low plasma β compared to the background solar wind. Therefore, the ejecta should be an MFR structure, which is also supported by the presence of the bidirectional electrons (BDEs), as shown in panel (a), especially in the former part of the MC. Note that BDEs within the MFR have been regarded as the evidence to support that both footpoints of the MFR may still anchor on the Sun (e.g., Kilpua et al. 2013; Song et al. 2015).

The average Fe charge state in the MC is apparently elevated compared to the background solar wind and the sheath region as shown in panel (f) with the red line, which is a common phenomenon for MCs (e.g., Kilpua et al. 2013). The iron charge distribution has been used as an identifier of ICMEs (Lepri et al. 2001) because the high ionized iron was likely produced in the current sheet connecting the MFR/HC and the flare loops through magnetic reconnection and then filled in the MFR/HC (e.g., Ko et al. 2013). Therefore, the ion charge state offers an important clue to relating the MC and HC as its distribution is fully established within a few solar radii from the Sun and remains frozen after that (e.g., Esser & Edgar 2001; Chen et al. 2004).
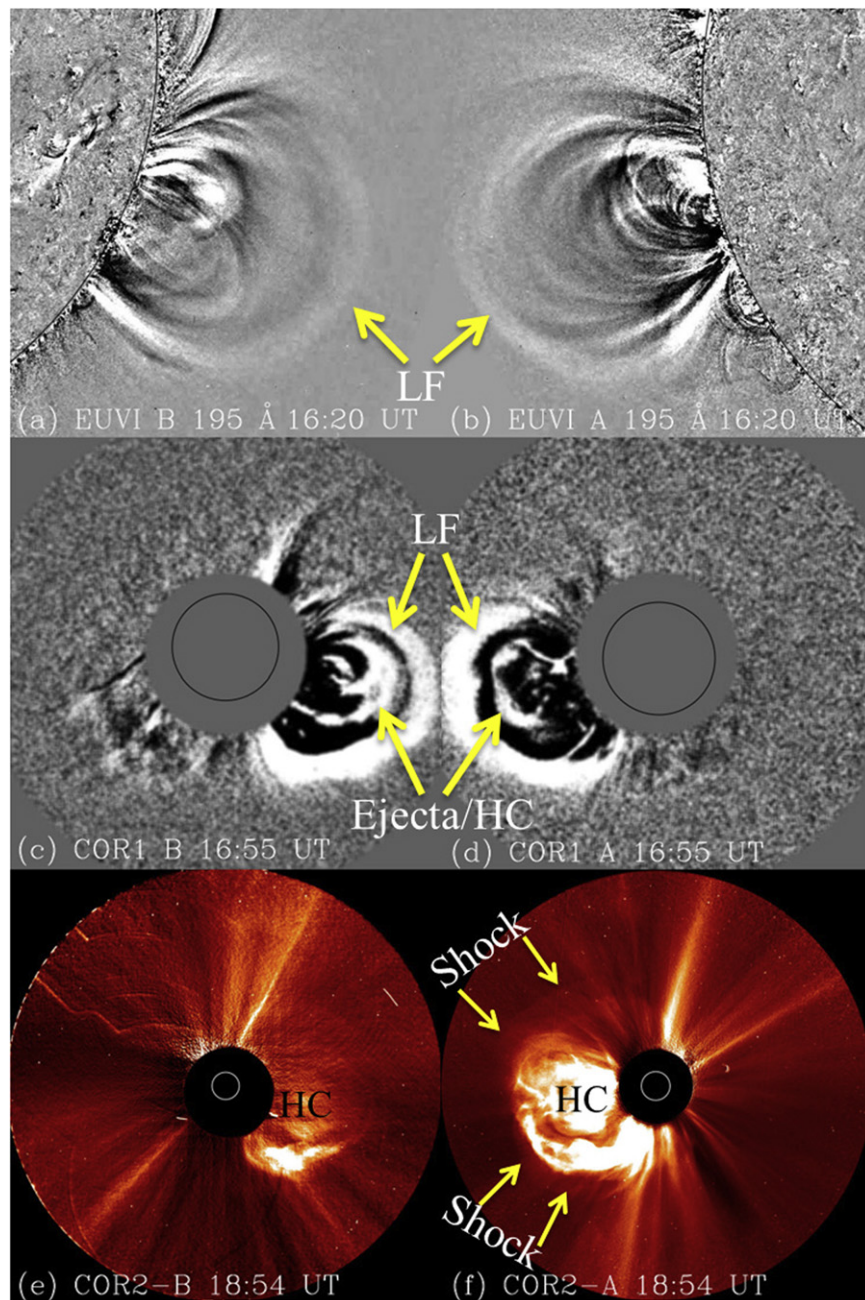
Figure 2. (a), (b) EUVI difference images of *STEREO* B and A. (c), (d) COR1 difference images of the CME. (e), (f) COR2 direct images of the CME. (Animations a and b of this figure are available.)

As described above, the erupted HC existed prior to the flare onset with a relative lower temperature ($\sim$5 MK). As the reconnection takes place along the post-CME current sheet, the preexisting HC structure will add more layers of plasma with the reconnected field lines, and the heated plasma will fill in the HC structure like "layers of an onion" (Lin et al. 2004; Ko et al. 2013). Therefore, we would expect to observe an MC with elevated Fe charge state, containing a relatively low-ionization-state center and a high-ionization-state shell for this event, which is confirmed by the observations as shown in panel (f). The average Fe charge state near the MC center is close to 10.5+, apparently lower than those at the shell (beyond 12+), but slightly higher than the background solar wind (below 10+) as the HC prior to the eruption had a higher temperature ($\sim$5 MK) than the background solar wind ($\sim$1–2 MK) in the corona. Note the background average Fe charge state is depicted with the blue dotted line. For the filaments contained in ICMEs, their in situ average ion charge states might be lower than those in the background solar wind (Lepri & Zubruchen 2010; Ko et al. 2013), as their initial temperatures in the corona are lower than their backgrounds, which does not conflict with our observations. Our average Fe charge state observations are qualitatively consistent with the expectation, which provides further support that the MC is the interplanetary counterpart of the erupted HC in the corona for this event. Note the preexisting HC will grow up during the eruption, and the MC corresponds to the final HC after the flare reconnection. Therefore, the preexisting HC should correspond
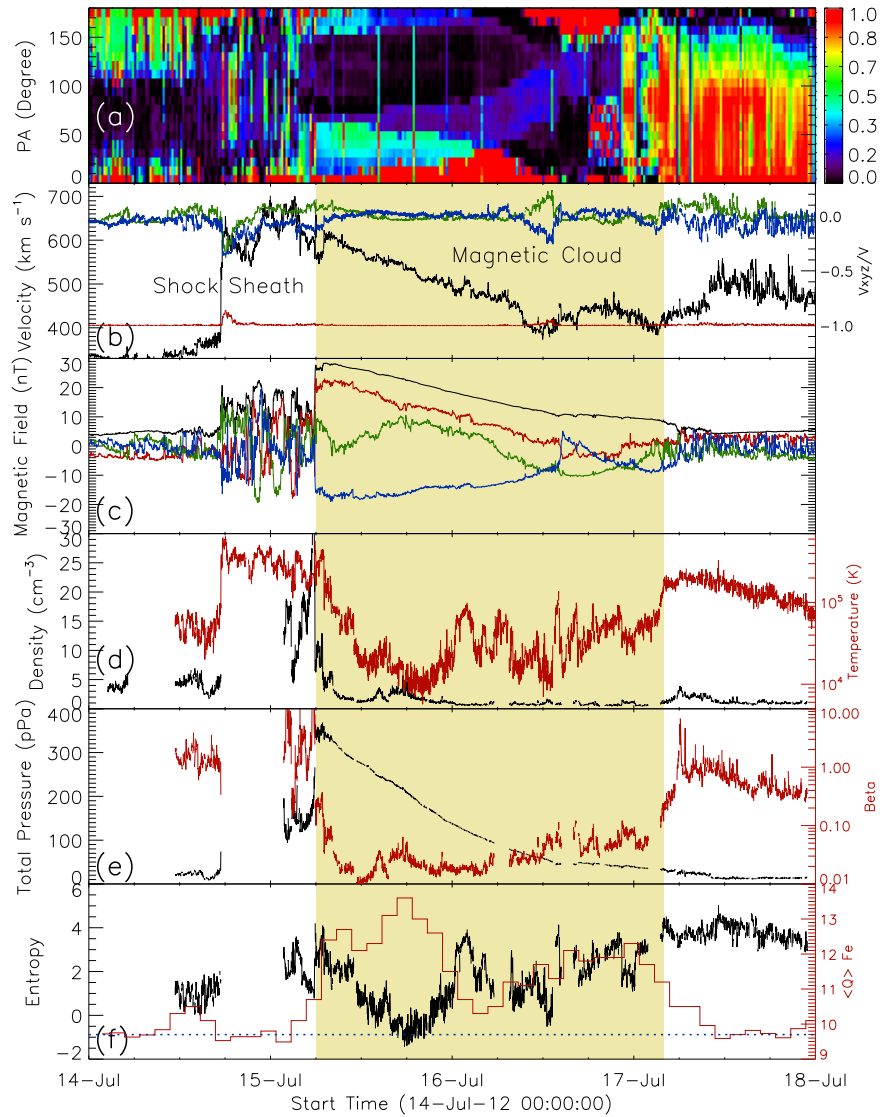
Figure 3. Solar wind parameters measured with *ACE*. From top to bottom, the panels show the PAD of electrons at 272 eV, bulk speed, magnetic field, density and temperature, plasma β, and total pressure, as well as entropy and average Fe charge state.

to the central part of the MC. Unfortunately, as the SWICS on board *ACE* suffered a hardware anomaly in 2011 and lost the ability to provide reliable iron charge state distributions, no quantitative temperature analysis is provided based on the charge state distributions.

4. DISCUSSION

Song et al. (2015) identified the counterpart of an HC in interplanetary space for the first time through analyzing its high temperature, appearance behind the shock and sheath, and the associated BDEs. They suggested that the HC will not evolve into a typical MC with low temperature under some special conditions. For instance, if there exists a corotating interaction region (CIR) ahead of the HC, then the CIR can form a magnetic container to inhibit the expansion of the HC and cool it down to a low temperature, which is the case reported in Song et al. (2015). They also showed that the spacecraft passed far away from the HC center, so no regular rotations of magnetic field components were observed. Therefore, they did not give strong evidence to support that the HC is the MFR.

However, the present event shows a pure ICME event, and there is not a CIR structure interacting with the ICME according to the in situ observations. Therefore, the HC can expand freely and evolve into a low-temperature and low-density structure during its propagation to ~1 AU.

MCs are detected in only about 30% of ICMEs (Richardson & Cane 2010; Wu & Lepping 2011). Riley & Richardson (2013) summarized the factors to explain why some ICMEs are observed to be MCs and others are not, including (1) the observational selection effect of ICMEs, (2) the different initiation mechanisms of CMEs, (3) the interactions of an MFR with itself or between neighboring MFRs, and (4) the different evolutionary processes of MFRs. Based on our present study and Song et al. (2015), we support that the evolutionary process plays an important role on whether an HC will form an MC during its propagation to ~1 AU, and the process can be greatly influenced by the interactions between the CME and CIR.

Song et al. (2014b) demonstrated that an HC's temperature was around 5 MK prior to the eruption and increased to ~9 MK at the flare peak, accompanying the growth of its volume. We

suggest that the heating process is likely to wear a higher temperature "coat" for the preexisting HC through magnetic reconnection. The preexisting HC might keep its original relative lower temperature. Ciaravella & Raymond (2008) pointed out that the temperature in the current sheet can reach a maximum value of ~8 MK in an event, approaching the coat temperature of the HC and supporting our explanation. The low-temperature "body" and high-temperature "coat" of the erupted HC might correspond to the low-ionization-state center and high-ionization-state shell of the MC.

5. SUMMARY

An HC erupted on 2012 July 12, accompanying an X1.4 class SXR flare and a CME. The high-temperature images of AIA showed that the HC existed prior to the eruption and recorded its whole eruption process. The EUVI and COR on board *STEREO* recorded the eruption edge-on. The low-temperature images of EUVI only showed the cooler LF ahead of the ejecta, while COR images can present both the LF and the ejecta. These are consistent with the high temperature and high density of the HC structure and support that the ejecta corresponds to the erupted HC. Meanwhile, the associated CME shock ahead of the sheath region and the ejecta was identified through the COR2 images, and these three structures were clearly detected with the in situ data sequentially when the associated ICME passed through *ACE*. The ejecta evolved into an MC with elevated Fe charge state, containing a relatively low-ionization-state center and a high-ionization-state shell, which was consistent with the preexisting MFR observation and its growth process through magnetic reconnection. All of these observations support that the MC structure detected by *ACE* is the counterpart of the erupted HC in the lower corona and the preexisting HC corresponds to the central part of the MC structure. Therefore, our study provided strong observational evidence that the HC in the lower corona is an MFR.

REFERENCES

Burlaga, L., Sittler, E., Mariani, F., & Schwenn, R. 1981, JGR, 86, 6673
Chen, P. F. 2011, LRSP, 8, 1
Chen, Y., Esser, R., Strachan, L., & Hu, Y. 2004, ApJ, 602, 415
Cheng, X., Ding, M. D., Guo, Y., et al. 2014a, ApJ, 780, 28
Cheng, X., Ding, M. D., Zhang, J., et al. 2014b, ApJL, 789, L35
Cheng, X., Ding, M. D., Zhang, J., et al. 2014c, ApJ, 789, 93
Cheng, X., Zhang, J., Ding, M. D., Liu, Y., & Poomvises, W. 2013, ApJ, 763, 43
Cheng, X., Zhang, J., Liu, Y., & Ding, M. D. 2011, ApJL, 732, L25
Cheng, X., Zhang, J., Saar, S. H., & Ding, M. D. 2012, ApJ, 761, 62
Ciaravella, A., & Raymond, J. C. 2008, ApJ, 686, 1372
Del Zanna, G., O'Dwyer, B., & Mason, H. E. 2011, A&A, 535, A46
Esser, R., & Edgar, R. J. 2001, ApJ, 563, 1055
Feng, S. W., Chen, Y., Kong, X. L., et al. 2012, ApJ, 753, 21
Feng, S. W., Chen, Y., Kong, X. L., et al. 2013, ApJ, 767, 29
Gloeckler, G., Cain, J., Ipavich, F. M., et al. 1998, SSRv, 86, 497
Gosling, J. T., McComas, D. J., Phillips, J. L., & Bame, S. J. 1991, JGR, 96, 7831
Hess, P., & Zhang, J. 2014, ApJ, 792, 49
Howard, R. A., Moses, J. D., Vourlidas, A., et al. 2008, SSRv, 136, 67
Kilpua, E. K. J., Isavnin, A., Vourlidas, A., Koskinen, H. E. J., & Rodriguez, L. 2013, AnGeo, 31, 1251
Ko, Y.-K., Raymond, J. C., Rakowski, C., & Rouillard, A. 2013, in AIP Conf. Ser. 1539, SOLAR WIND 13: Proceedings of the Thirteenth International Solar Wind Conference, ed. G. P. Zank et al. (Melville, NY: AIP), 207
Lemen, J. R., Title, A. M., Akin, D. J., et al. 2012, SoPh, 275, 17
Lepri, S. T., & Zubruchen, T. H. 2010, ApJL, 723, L22
Lepri, S. T., Zurbuchen, T. H., Fisk, L. A., et al. 2001, JGR, 106, 29231
Lin, J., Raymond, J. C., & van Ballegooijen, A. A. 2004, ApJ, 602, 422
McComas, D. J., Bame, S. J., Barker, P., et al. 1998, SSRv, 86, 563
McKenzie, D. E., & Canfield, R. C. 2008, A&A, 481, L65
Möstl, C., Amla, K., Hall, J. R., et al. 2014, ApJ, 787, 119
O'Dwyer, B., Del Zanna, G., Mason, H. E., Weber, M. A., & Tripathi, D. 2010, A&A, 521, A21
Patsourakos, S., Vourlidas, A., & Stenborg, G. 2013, ApJ, 764, 125
Richardson, I. G., & Cane, H. V. 2010, SoPh, 264, 189
Riley, P., & Richardson, I. G. 2013, SoPh, 284, 217
Rust, D. M., & Kumar, A. 1994, SoPh, 155, 69
Shen, F., Shen, C., Zhang, J., et al. 2014, JGRA, 119, 7128
Smith, C. W., L'Heureux, J., Ness, N. F., et al. 1998, SSRv, 86, 613
Song, H. Q., Zhang, J., Chen, Y., & Cheng, X. 2014a, ApJL, 792, L40
Song, H. Q., Zhang, J., Chen, Y., et al. 2015, ApJ, 803, 96
Song, H. Q., Zhang, J., Cheng, X., et al. 2014b, ApJ, 784, 48
Titov, V. S., & Démoulin, P. 1999, A&A, 351, 707
Vourlidas, A., Lynch, B. J., Howard, R. A., & Li, Y. 2013, SoPh, 284, 179
Vourlidas, A., Wu, S. T., Wang, A. H., Subramanian, P., & Howard, R. A. 2003, ApJ, 598, 1392
Wang, Y.-M., & Stenborg, G. 2010, ApJL, 719, L181
Wu, C.-C., & Lepping, R. P. 2011, SoPh, 269, 141
Zhang, J., Cheng, X., & Ding, M.-D. 2012, NatCo, 3, 747
Zhang, J., Dere, K. P., Howard, R. A., & Bothmer, V. 2003, ApJ, 582, 520
Zhang, J., Richardson, I. G., Webb, D. F., et al. 2007, JGRA, 112, A10102